

Brillouin study of acoustic modes in isotropic, smectic-A, and smectic-C* phases in a ferroelectric liquid crystal

P. Kužel,^{1,*} C. Dugautier,¹ M. Pavel,² and P. Moch¹

¹*Laboratoire des Propriétés Mécaniques et Thermodynamiques des Matériaux, CNRS, Institut Galilée, Université Paris-Nord, 93430 Villetaneuse, France*

²*Institute of Physics, Academy of Sciences of the Czech Republic, Na Slovance 2, 180 40 Prague 8, Czech Republic*

(Received 12 January 1996; revised manuscript received 17 May 1996)

This work concerns the study of collective modes in a smectic liquid crystal in the hypersonic frequency range. Special attention is paid to the determination of the significant anisotropy of the quasilongitudinal mode and to its temperature dependence, namely, near the isotropic–smectic-A phase transition. The interpretation is provided in terms of the pseudocrystalline model by means of effective stiffness and viscosity tensors. A weak quasitransverse mode has been detected: the angular variations of its frequency and of its intensity are in good agreement with the predictions of our model. We confirm a universal behavior for nematic and smectic phases at high frequencies: in the hypersonic regime the orientational order of the molecules seems to play a more important role than the smectic ordering. A quantitative analysis of the angular and temperature dependence of the inelastically scattered intensity is done: the observed intensity anomalies are well described by our model. The smectic-C*–smectic-A phase transition is investigated by means of Brillouin scattering: only very small anomalies are found. [S1063-651X(96)01512-7]

PACS number(s): 64.70.Md, 78.35.+c, 62.20.Dc, 77.84.Nh

I. INTRODUCTION

Up to now the elastic properties of liquid crystals are not completely understood and the strong frequency dependencies are explained only qualitatively. Generally, two approaches can be used: the first one is based on a hydrodynamic treatment generalizing the hydrodynamics of isotropic fluids by introducing suitable additional variables responsible for the anisotropy [1–3]: such a model can be developed for smectic and nematic liquid crystals but does not predict any changes in elastic properties of nematic phases with regard to the isotropic phase [4]. The second approach is a phenomenological pseudocrystalline model using an elastic stiffness tensor appropriate to the symmetry and taking into account the vanishing of some shear constants of the studied liquid crystalline phase. It should be noted that for smectics the use of a phenomenological elastic stiffness tensor is completely justified by a hydrodynamic calculation that allows one to evaluate the elastic stiffness components [4].

However, the experimental results are less convincing since, in the hypersonic regime, which is studied by means of Brillouin scattering, smectic and nematic liquid crystals show nearly the same elastic properties [5,6]. This fact supports the hypothesis that the hydrodynamic approach is not valid here and that a universal interpretation, which presently is still lacking, should exist for both types of liquid crystals. On the other hand, the problem of the existence of a shear-like acoustic mode is not yet completely resolved. It has been

experimentally observed once in smectics [7] but, in spite of considerable effort, it has not been detected in nematics up to now [5].

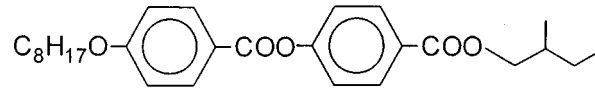
The results found in the ultrasonic regime depend on the material used and on the frequency range studied. Frequently, the nematic liquid crystals show, at low ultrasonic frequencies, an anisotropy of the damping while the propagating velocity remains isotropic [for example, this is the case of *p*-azoxyanisole (PAA) at 10 MHz [8] or of *p*-methoxybenzylidene *p*-(*n*-butylaniline) (MBBA) at 23 MHz [9]]. In contrast, the nematic phase of terephthal-*bis-p-p'*-butylaniline (TBBA) at 2 MHz behaves practically like an isotropic liquid [10]. For nematic MBBA and CBOOA [11,12], the studies of the anisotropies in a broad frequency range reveal the existence of at least one relaxation process that causes an increase of the elastic stiffness anisotropy at high frequency. Concerning the smectic phases, a significant anisotropy of the elastic properties is always observed by means of ultrasounds [10,13–15].

Most of the published Brillouin studies [5,11] concern liquid crystals showing an isotropic↔nematic phase transition (in some cases followed by a nematic↔smectic one). We found it interesting to compare this case to the situation where the studied compound directly undergoes an isotropic↔smectic transition. Only a very few Brillouin experiments have been performed concerning transitions between distinct smectic or smectic-hexatic phases. Our compound shows a smectic-A↔smectic-C* transition. In this paper we discuss the Brillouin spectra of a smectic liquid crystal and we derive conclusions about its elastic properties and about their anomalies in the vicinity of its phase transitions.

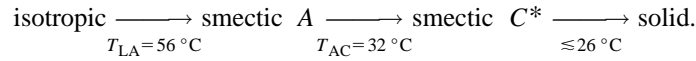
II. EXPERIMENTAL DETAILS

In our experiments we used the 4-*n*-octyloxy benzoic acid 4'-[(2-methyl butyloxy) carbonyl] phenyl ester:

*Corresponding author. Present address: Institute of Physics, Academy of Sciences of the Czech Republic, Na Slovance 2, 180 40 Prague 8, Czech Republic.



which exhibits the following phase transitions [16]:



It should be noted that we observed the isotropic–smectic-*A* phase transition at slightly lower temperature (54–55 °C) than that previously reported.

The studied samples filled the space between two glass plates (separated by 25 μm) with indium-tin oxide electrodes on the inner surface. The glass electrodes were previously coated with a polyimide layer conveniently rubbed with a velvet cloth to favor the planar alignment. By applying an ac electric field (1–10 Hz, 100 V) near the smectic-*C**–smectic-*A* transition temperature during a period of several hours the alignment was improved, resulting in parallel smectic layers perpendicular to the glass plates. The alignment was controlled during the scattering measurements by checking the diffraction pattern (which forms a well-defined stripe in the aligned state) of the transmitted laser beam.

A home-made furnace allowing rotations around the axis normal to the films was used: the temperature of the scattering volume was determined with a precision of 1 °C. It was possible to apply a dc or an ac electric field during the Brillouin measurements.

The chosen 90° geometrical arrangement with plates bisecting the angle between the incident and the scattered beam (Fig. 1) provides complete anisotropy measurements. The resulting phonon frequencies are practically independent of the refractive indices [17,18] at least in the case of an axial symmetry around the *z* axis normal to the smectic layers (smectic-*A* phase).

The Brillouin experiments were performed using a 2×3 passes tandem Fabry-Pérot interferometer. The samples were illuminated by a single-mode argon ion laser at a wavelength of 5145 Å, using powers not exceeding 35 mW in order to avoid damage of the sample caused by laser-induced flows of matter. We checked that the lowering of the laser power down to a few mW had no influence on the measured spectra. We encountered some difficulties when measuring the spectra just below the isotropic–smectic-*A* transition (52–55 °C) where the electrical field of the laser beam causes flows of matter that become apparent through fast chaotic changes in the diffraction pattern and that can destroy the molecular alignment or result in a damage of the sample. Consequently, there is a large scattering of the experimental points in this temperature range. The full width at half maximum (FWHM) of the instrumental function was of about 110 MHz for the free spectral range used (for most experiments the frequency distance between the central line and the first maximum ghost was about 0.27 cm^{-1} , e.g., 8.2 GHz) and it was very small compared to the width of the observed Brillouin

lines (between 700 and 1100 MHz, depending upon the temperature and the propagation direction). This free spectral range was found to be the most convenient for the study of both quasilongitudinal (QL) and quasitransverse (QT) modes: we lose the finesse and the signal when lowering it significantly.

III. RESULTS AND DISCUSSION

A. Theoretical background–phenomenological treatment

Our theoretical description is based on a formalism that is conventionally employed in the discussion of elastic properties of crystals. We suppose that the coupling of the acoustic modes to other vibrational and relaxational modes is well described by a renormalization of the effective stiffness and viscosity coefficients as is most frequently the case [11]. If this condition is not valid it is necessary to write down explicitly the coupled equations and calculate the spectral density that can differ significantly from the harmonic oscillator spectral function [19].

The sound propagation in solids can be described by a displacement vector \vec{u} that satisfies the equation of motion:

$$\rho_0 \ddot{u}_i = C_{ijkl} \frac{\partial^2 u_k}{\partial x_j \partial x_l} - \eta_{ijkl} \frac{\partial^2 \dot{u}_k}{\partial x_j \partial x_l}, \quad (1)$$

where the symmetry properties of the viscosity tensor η_{ijkl} and of the elastic stiffness tensor C_{ijkl} are the same as follows from the Onsager theorem, and where ρ_0 is the mass density. By analogy, we shall use the same equation of motion for the phenomenological description of the acoustic modes in liquid crystals. We are aware that the three-component displacement vector \vec{u} is only a hypothetical parameter in liquid crystalline phases and that it does not have a clear physical meaning. However, one can define it formally through the implicit relation $v_i = \partial u_i / \partial t$, where v_i is a

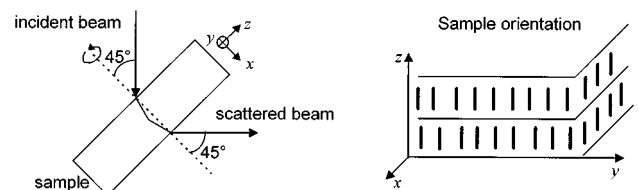


FIG. 1. Schematic view of the scattering geometry.

component of the flow velocity. It is then possible to solve Eq. (1) for the formal variable \vec{u} or to rewrite this equation for the flow velocity \vec{v} .

In the smectic-A phase there are five independent viscosity coefficients, $\eta_{11}(=\eta_{22})$, η_{33} , $\eta_{13}(=\eta_{23})$, $\eta_{55}(=\eta_{44})$, and η_{66} ($\eta_{12}=\eta_{11}-2\eta_{66}$), in comparison with the two independent coefficients of the isotropic liquid phase (η_{11} and η_{66}). Assuming that the shear stiffness coefficients vanish, there are three independent stiffness constants in the smectic phases, $C_{11}(=C_{22}=C_{12})$, $C_{13}(=C_{23})$, and C_{33} , to compare to the single one in the isotropic liquid phase. In the case of small viscosities, the dispersion relations do not depend upon η up to second order and one finds two propagation modes (+ and -) with frequencies $\omega_{\pm}=k\sqrt{C_{\pm}/\rho_0}$ where

$$C_{\pm} = \frac{1}{2}[C_{11}\sin^2\varphi + C_{33}\cos^2\varphi \pm \sqrt{(C_{11}\sin^2\varphi - C_{33}\cos^2\varphi)^2 + C_{13}^2\sin^2 2\varphi}]. \quad (2)$$

In expression (2), φ is the angle between the wave vector \vec{k} and the z axis. Assuming that C_{11} , C_{13} , and C_{33} are not extremely different the “+” mode is quasilongitudinally polarized while the “-” mode is quasitransversally polarized. We introduce a parameter α which expresses the degree of the longitudinality of the quasitransverse mode:

$$\frac{u_{\parallel}^+}{u_{\perp}^+} = -\frac{u_{\perp}^-}{u_{\parallel}^-} = \frac{1}{\alpha}, \quad (3)$$

where u_{\parallel} is the projection of the displacement vector \vec{u} on the wave-vector direction \vec{k}/k ; $\vec{u}_{\perp} = \vec{u} - \vec{u}_{\parallel}$. One finds

$$\alpha = \frac{C_{13}\cos^2\varphi - (C_{+} - C_{11}\sin^2\varphi) \sin\varphi}{C_{13}\sin^2\varphi + (C_{+} - C_{11}\sin^2\varphi) \cos\varphi}. \quad (4)$$

The Brillouin intensity of an observed mode is proportional to the imaginary part of the elastic susceptibility and can be fitted by the damped harmonic-oscillator spectral function:

$$S(\omega_{\pm}) \propto \frac{1}{(\omega^2 - \omega_{\pm}^2)^2 + \omega^2 \gamma_{\pm}^2}, \quad (5)$$

where $\gamma_{\pm} = k^2 \eta_{\pm} / \rho_0$ represents the FWHM of the Brillouin lines. As follows from the solution of Eq. (1):

$$\eta_{+} = \eta_{33}\cos^4\varphi + \eta_{11}\sin^4\varphi + 2(2\eta_{55} + \eta_{13})\sin^2\varphi \cos^2\varphi, \quad (6a)$$

$$\eta_{-} = \eta_{55} + (\eta_{11} + \eta_{33} - 2\eta_{13} - 4\eta_{55})\sin^2\varphi \cos^2\varphi. \quad (6b)$$

The k value is fixed by the experimental setup ($k = \sqrt{2}\omega_i/c$, where ω_i is the radial frequency of the incident light; in our case $k = 1.73 \times 10^5 \text{ cm}^{-1}$). Expressions (5) and (6a and 6b) are strictly valid only if $\omega_{\pm}^2 \gg \gamma_{\pm}^2$; in general, they can be used even when $\omega_{\pm} \gtrsim 3\gamma_{\pm}$.

Note that ω_{\pm} and η_{\pm} do not vary in the same way versus φ . From the φ dependence of ω_{+} or ω_{-} it is possible to derive C_{11} , C_{13} , and C_{33} . From the variation of γ_{+} or γ_{-} versus φ it is then possible to determine η_{11} , η_{33} , and $(\eta_{13} + 2\eta_{55})$.

In order to evaluate the intensity one can use a phenomenological pseudocrystalline model by introducing a four-

rank photoelastic tensor p_{ij} (in Voigt notation) appropriate to the axial symmetry, equivalent to the hexagonal one, with $p_{44} = p_{55} = p_{66} = 0$. The intensity of the scattered light is then given by [20,21]

$$I^{\mu\mu'}(\vec{k}) \propto \left[\frac{e_{\mu,j} e'_{\mu',i} \epsilon_{ii'} \epsilon_{jj'} p'_{i'j'lm} u_l k_m}{v} \right]^2, \quad (7)$$

\vec{e} , \vec{e}' are the unit polarization vectors of the incident and scattered light, respectively. The indices μ and μ' refer to the beam polarization (ordinary or extraordinary). ϵ_{ij} is the high-frequency dielectric permittivity tensor, u_l are the components of the displacement vector obtained from Eq. (1), \vec{k} is the phonon wave vector and v is its propagation velocity given through Eq. (2).

In our experiments, the scattered light was not polarized and the polarization of the incident beam was held fixed in the laboratory frame: it means that it turned in the sample frame (cf. Fig. 1). Taking into account the geometry of the experiment and ignoring nearly negligible birefringence effects, it follows from expression (7) that the light intensity scattered from the QL and QT mode is proportional to

$$I_{\pm}(\varphi) \propto \frac{1}{C_{\pm}(\varphi)} \left[\sin^2\varphi (p_{33}u_3^{\pm}k_3 + p_{31}u_1^{\pm}k_1)^2 + \cos^2\varphi (p_{11}u_1^{\pm}k_1 + p_{13}u_3^{\pm}k_3)^2 - \frac{1}{2n^2} \times [(p_{33} - p_{13})u_3^{\pm}k_3 + (p_{31} - p_{13})u_1^{\pm}k_1]^2 \times \sin^2\varphi \cos^2\varphi, \right] \quad (8)$$

where n is the mean refractive index. We recall that the indexes 1 and 2 are strictly equivalent. If the coefficients p_{ij} are close to each other, the third term of expression (8) is negligible with regard to the sum of the first and second ones. Notice that in the liquid isotropic phase all the p_{ij} are identical for $i \leq 3$ and $j \leq 3$. In this case expression (8) is φ independent as expected.

Formula (8) is rather complicated and the intensity anisotropy depends on three unknown variables (ratios of p_{ij}). Analytical investigation of its behavior is thus very difficult. In addition, Brillouin scattering experiments using a piezo-scanned interferometer do not allow very precise measurements of the intensities of acoustic phonons, especially when, as in our case, the orientation of the sample has to be modified between two consecutive measurements and when the scattered intensity is low. With careful experiments the precision does not exceed 20%–30%. It follows that the complete set of the photoelastic coefficients cannot be experimentally obtained with sufficient accuracy. In solid crystals, the values of the implied photoelastic coefficients do not usually markedly differ from each other and a good qualitative picture is obtained supposing $p_{13} \approx p_{11}$ and $p_{31} \approx p_{33}$. Although we cannot *a priori* justify this approximation in the case of liquid crystals, we use it. We show below that it gives a good account of the intensity anisotropy of the QL mode and predicts qualitatively the behavior of the QT mode. The improvement of the model obtained when slightly modifying p_{11} and p_{33} is considered. The problem is revisited in the discussion.

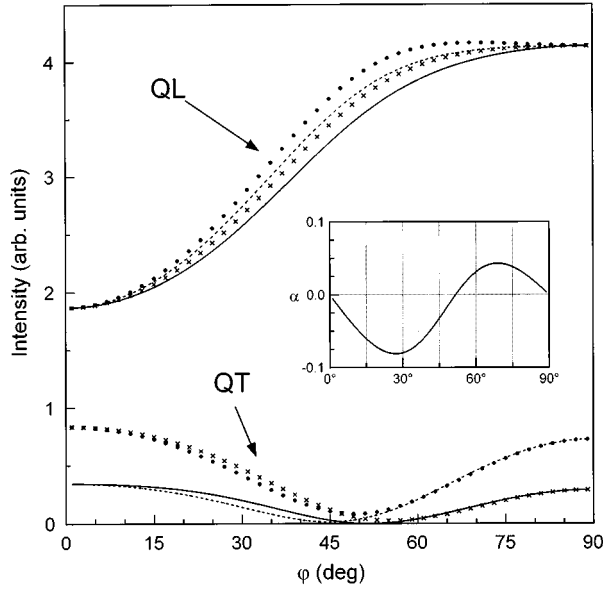


FIG. 2. Simulation of the intensity variation of the QL and QT modes based on expression (8). Inset: angular variation of the parameter α defined by expressions (3) and (4). The values of C_{ij} are given in the legend of Fig. 9. Parameters: $p_{31}/p_{13}=1.4$ (typical value for our sample). (—) $p_{11}=p_{13}$, $p_{33}=p_{31}$ [in this case the expression (8) can be simplified and replaced by (9)]; (xxx) $p_{11}=1.15p_{13}$, $p_{33}=p_{31}$; (---) $p_{11}=p_{13}$, $p_{33}=1.1p_{31}$; (···) $p_{11}=1.15p_{13}$, $p_{33}=1.1p_{31}$.

Taking into account these simplifying equalities and using the condition $\alpha^2 \ll 1$ (see above and the inset in Fig. 2), one finds for the intensities of the QL and of the QT mode:

$$I_+ \propto \frac{1}{C_+} \left(p_{13}^2 \cos^2 \varphi + p_{31}^2 \sin^2 \varphi - \frac{1}{2n^2} (p_{31} - p_{13})^2 \sin^2 \varphi \cos^2 \varphi \right), \quad (9a)$$

$$I_- \propto \frac{\alpha^2}{C_-} \left(p_{13}^2 \cos^2 \varphi + p_{31}^2 \sin^2 \varphi - \frac{1}{2n^2} (p_{31} - p_{13})^2 \sin^2 \varphi \cos^2 \varphi \right), \quad (9b)$$

and, consequently

$$\frac{I_-}{I_+} = \alpha^2 \frac{\omega_+^2}{\omega_-^2}. \quad (10)$$

This means that only the longitudinal part of the mode vibrations contributes to the scattered intensity. α and ω_- are strongly φ dependent while ω_+ only weakly varies upon φ [cf, Eqs. (2) and (4)] and, due to the large experimental errors in the intensity measurements, can be often considered as constant. Since α remains small compared to 1 and even to ω_-^2/ω_+^2 , I_- is expected to be significantly smaller than I_+ .

The QT mode becomes purely transverse ($\alpha=0$) for an angle φ_L defined by the equation

$$\tan \varphi_L = \left(\frac{C_{33} - C_{13}}{C_{11} - C_{13}} \right)^{1/2}; \quad (11)$$

for this angle the intensity I_- defined by formula (9b) vanishes. Generally, in liquid crystals one experimentally finds that $C_{33} > C_{11}$ and consequently $\varphi_L > 45^\circ$. This fact is the starting point of our interpretation of the rather surprising intensity variation of the QT mode intensity.

Figure 2 shows clearly the meaning of all the nonzero photoelastic coefficients: the ratio p_{31}/p_{13} is set to a value typical for our sample and we study the changes in the angular intensity variation when p_{11} and p_{33} are modified by about 10%. The value of the QL intensity depends practically only upon p_{13} and p_{31} : the changes introduced by the simultaneous or separate modifications of p_{11} and p_{33} are very small and cannot be detected by means of Brillouin scattering. The curves corresponding to the intensity variation of the QT mode show a minimum near φ_L . The value of the coefficient p_{11} influences only the left part of the curve ($\varphi < \varphi_L$) while the coefficient p_{33} modifies only the right part of the curve ($\varphi > \varphi_L$). It should be noticed that the predictions of our model relative to the QT mode are not valid for angles close to 0 or $\pi/2$: either the mode becomes overdamped and the approach based on expression (7) cannot be applied ($\omega_- < \gamma_-$) or there is some small but nonzero value of C_{44} that can originate from a small imaginary part of the viscosity and that leads to a zero value of I_- for $\varphi=0$ and $\pi/2$.

B. Analysis of the experimental results

1. Quasilonitudinal mode

We first discuss the results relative to the quasilonitudinal (QL) mode. The obtained spectra are well fitted with a

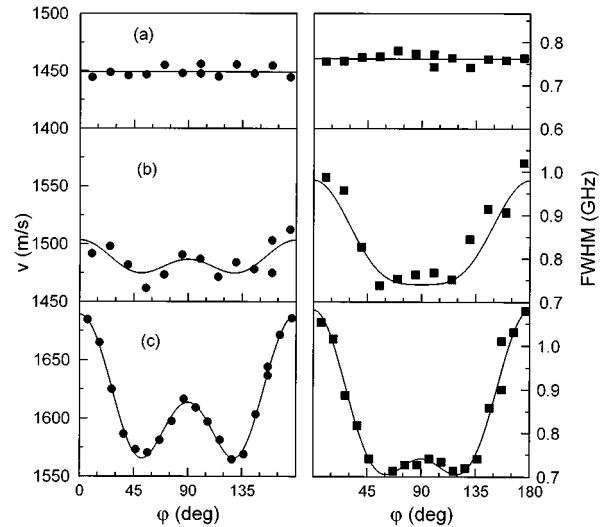


FIG. 3. Angular variation of the propagating velocity (left column) and of the width of the Brillouin lines (right column) relative to the quasilonitudinal mode for three different temperatures. (a) Just above the isotropic–smectic-A transition ($T=55^\circ\text{C}$); (b) near below this transition ($T=50^\circ\text{C}$); (c) deep in the smectic phase ($T=33^\circ\text{C}$). The solid curves are fits with the expressions (2) and (6a); in the isotropic phase the horizontal straight line represents the mean value.

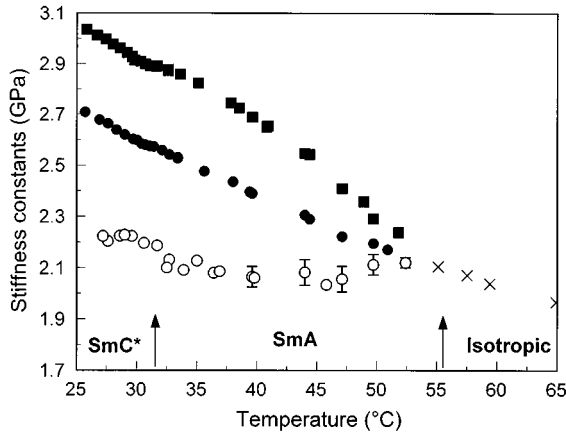


FIG. 4. Variation of the stiffness constants versus temperature: (\times) C_0 in the isotropic phase, (\bullet) C_{11} , (\blacksquare) C_{33} , and (\circ) C_{13} . The plotted values were calculated using a mass density of 1000 kg/m^3 , which certainly does not differ much from the actual value of ρ_0 (nonmeasured).

sum of a zero-centered Lorentzian function and a harmonic-oscillator spectral function (5) (see Fig. 8a below). We have measured the temperature dependence of the angular variation of the propagation velocity and of the damping. It is interesting to compare the results obtained in the smectic phase well below and near below the smectic-isotropic transition at T_{LA} with the data relative to the isotropic phase just above this transition (Fig. 3). In the smectic phase the results are well fitted with the theoretical expressions (2) and (6a); they provide the values of the three independent components of the elastic stiffness tensor (C_{11} , C_{13} , and C_{33}) and of three independent viscosity coefficients (η_{11} , η_{33} , and $\eta_{13}+2\eta_{55}$). As shown in Fig. 4, the anisotropy of the stiffness constants vanishes at T_{LA} and continuously develops when lowering the temperature. In contrast, the viscosity shows a marked discontinuity in η_{33} at T_{LA} (Fig. 5).

Finally, we have measured the variation of the QL-mode intensity. Figure 6 shows the difference between the angular variation of the intensity in the isotropic and the smectic-A

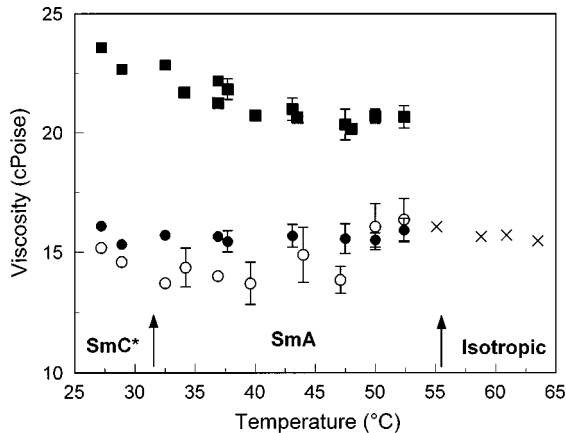


FIG. 5. Variation of the viscosity components versus temperature: (\times) viscosity in the isotropic phase, (\bullet) η_{11} , (\blacksquare) η_{33} , and (\circ) $\eta_{13}+2\eta_{55}$. The plotted values were calculated using a mass density of 1000 kg/m^3 .

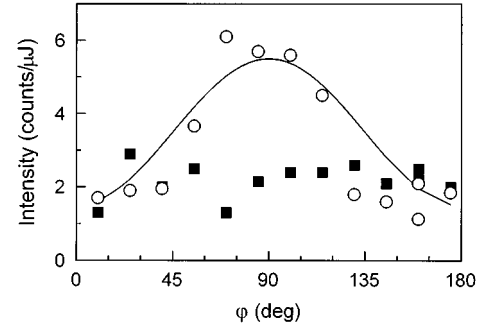


FIG. 6. Angular variation of the scattered intensity of the longitudinal mode in the isotropic phase at $55 \text{ }^\circ\text{C}$ (\blacksquare), and of the quasi-longitudinal mode in the smectic-A phase at $50 \text{ }^\circ\text{C}$ (\circ). Solid line: fit with expression (9a).

phase very close to the transition temperature. The experimental points in the smectic phase are fitted with the function given in Eq. (9a). As shown in this figure, in the smectic phase the intensity exhibits a rather strong anisotropy leading to a value of p_{31}^2/p_{13}^2 significantly larger than 1, which is the value in the isotropic phase. The ratio p_{31}^2/p_{13}^2 ranges between 2 and 3 in both smectic phases (see Fig. 7).

2. Quasitransverse mode

Deep in the smectic phases (about $20 \text{ }^\circ\text{C}$ or more below T_{LA}) a shoulder is observed on the wing of the quasielastic peak for φ ranging from about 20° to 50° , as shown in Fig. 8(a). We interpret this feature as a weak quasitransverse (QT) mode. The spectral characteristics of this mode can be obtained by subtracting the background from the measured spectra. We proceed as follows (see Fig. 8): First, we perform a simultaneous fit of the QL and elastic lines for $\varphi=0^\circ$ (the same fit as described at the beginning of Sec. III B 1). The elastic peak is much more intense than the QL line and the points corresponding to intensities largely beyond the shown vertical range are not available (protection of the photomultiplier); thus no quantitative information about the central line can be obtained from the fit. However, it is noteworthy that the value of its FWHM resulting from our fit is very close to the FWHM of the instrumental function. The obtained FWHM value of the elastic line is then fixed and used for fitting all the spectra measured at other angles. In Fig. 8(a) we show the fits for $\varphi=20^\circ$, 30° , and 45° . In the regions

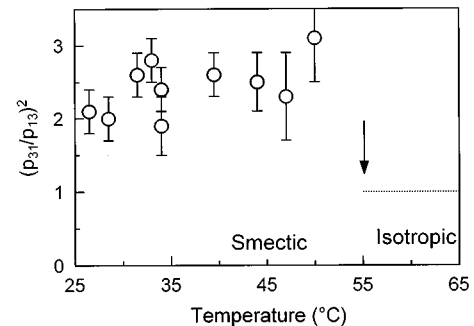


FIG. 7. Temperature dependence of the ratio of the photoelastic coefficients p_{31}^2/p_{13}^2 .

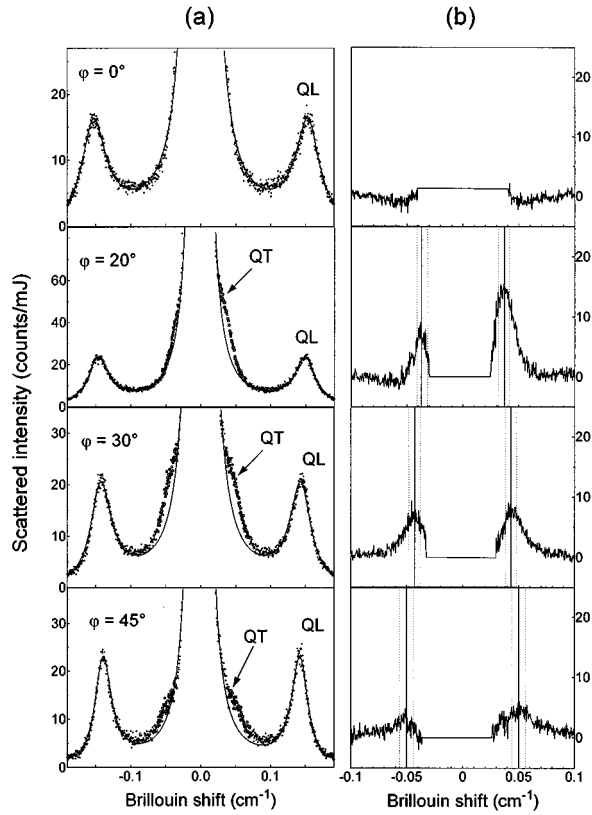


FIG. 8. (a) Examples of spectra at 33 °C for different angles φ between the direction of propagation and the normal to the layers. The shoulder on the wing of the quasielastic peak is assigned to the quasitransverse mode. Closed symbols: experimental data taken into account for the fit; open symbols: experimental data excluded for the fit; solid line: simultaneous fit of the central line and QL mode (see text). (b) Spectra of the QT mode obtained by a subtraction of the fit from the experimental data. Vertical solid and dotted lines correspond, respectively, to the values of the propagation velocity and to the error bars shown in Fig. 9.

where the intensity of the QT line is clearly nonzero the experimental points are not taken into account during the fitting procedure [open points in Fig. 8(a)]. The QT lines are then obtained by subtracting the fitted lines from the measured spectra. A very small asymmetry of the central line is found in some spectra (20°, 45°) yielding the fit less precise and resulting in a large difference between the intensities of the Stokes and anti-Stokes QT lines. The computed spectra of the QT mode are shown in Fig. 8(b) together with the values of the frequency used for the calculation of the propagation velocity (Fig. 9). However, the results of the fits should not be overestimated: the subtracted background varies very rapidly, its intensity is comparable or even superior to that of the QT line and, in addition, the instrumental function is slightly asymmetric for some spectra. In our opinion the fit yields a relatively good value for the propagation velocity, a rough estimate for the intensity variation and the order of magnitude for the FWHM.

Due to the limited angular interval and to the rather large uncertainty of the frequency determination, one cannot precisely evaluate C_{11} , C_{13} , and C_{33} from the measured spectra. However, as shown in Fig. 9, the QT velocities calculated from the stiffness constants derived using the QL-mode Brillouin data satisfactorily fit the experimental values. We recall that there is no extra fitting parameter and that the QT-mode propagation velocity is fully determined by the angular variation of the QL-mode frequency. This agreement justifies the theoretical treatment used in terms of elasticity tensors [Eq. (2)]. The FWHM of the QT mode has the expected order of magnitude and it seems to grow when 45° is approached as predicted by Eq. (6b), but it is not possible to derive quantitative conclusions about the behavior.

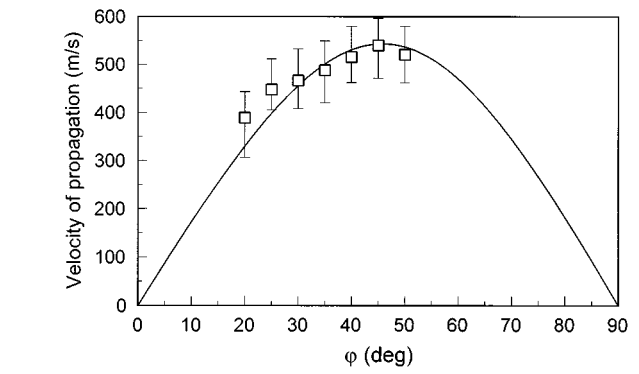


FIG. 9. Angular variation of the propagation velocity of the quasitransverse mode for $T=33$ °C. The solid line is obtained using the results of the fit of the QL-mode anisotropy at the same temperature [cf. Fig. 3(c)]: $C_{11}/\rho_0=2.61\times 10^6$ m²s⁻²; $C_{33}/\rho_0=2.89\times 10^6$ m²s⁻²; $C_{13}/\rho_0=2.16\times 10^6$ m²s⁻².

As expected, the scattered intensity is significantly smaller for the QT mode than for the QL mode. We recall that the QT mode becomes purely transverse for $\varphi=\varphi_L$: φ_L slightly depends upon the temperature and ranges between 50° and 55°. The measured intensity of the QT mode strongly depends of φ : it diminishes when φ increases from 20° to 50° and the spectral line is not observed for $\varphi>\varphi_L$ [Figs. 8(b) and 10(b)]. This evolution is qualitatively described by Eq. (9b). However, in order to obtain a quantitative agreement one has to take into account simultaneously the intensity variation of both modes. Figure 10 shows the intensity data obtained at 33 °C. The results relative to the QL mode [Fig. 10(a)] are fitted with the function (9a). The fit yields the values of p_{13} and p_{31} . Assuming that the simplified model is valid ($p_{11}=p_{13}$, $p_{33}=p_{31}$), one can predict the φ dependence of the ratio I_+/I_- . However, this prediction underestimates the measured values [cf., Fig. 10(b)]. The agreement can be significantly improved through an enhancement of p_{11} by about 25%: the φ dependence of I_+ changes only very slightly while I_-/I_+ is significantly increased for $\varphi<\varphi_L$.

However, our aim was not to quantitatively determine all the photoelastic coefficients. The experimental data do not allow it with a sufficient precision: the large error bars in Fig. 10(b) are related to the fact that one cannot exclude a systematic error in the QT intensity determination in spite of a careful fitting procedure. Our aim was to explain the rather surprising φ interval where the QT mode is observed: for $\varphi\lesssim 20^\circ$ the QT-mode frequency is very low and the line is merged in the quasielastic peak; assuming that p_{33} does not much exceed p_{31} , the intensity of the QT mode predicted by our model becomes very low for $\varphi\gtrsim 50^\circ$. To our knowledge, this QT mode has been observed only once [7] in a classical

louis data satisfactorily fit the experimental values. We recall that there is no extra fitting parameter and that the QT-mode propagation velocity is fully determined by the angular variation of the QL-mode frequency. This agreement justifies the theoretical treatment used in terms of elasticity tensors [Eq. (2)]. The FWHM of the QT mode has the expected order of magnitude and it seems to grow when 45° is approached as predicted by Eq. (6b), but it is not possible to derive quantitative conclusions about the behavior.

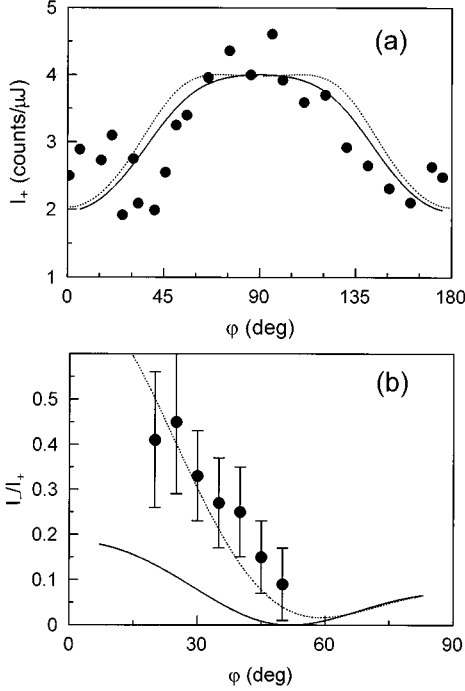


FIG. 10. (a) Angular variation of the intensity of the QL mode. (b) Angular variation of the intensity ratio I_-/I_+ of the QL and QT modes. Temperature: 33 °C; symbols: experimental values; solid line: simulation using Eq. (9) with $p_{31}=1.33p_{13}$; dotted line: simulation based on Eq. (8) and with $p_{33}=p_{31}=1.33p_{13}$, $p_{11}=1.25p_{13}$.

smectic structure, also in a restricted φ interval: we think that our interpretation of this narrow allowed interval of observation is more convincing than the previously reported one [22] based on an anomalous anisotropy of damping of the QT mode due to a coupling with a soft tilt-angle mode.

3. The smectic- C^* phase and the smectic- C^* -smectic- A transition

The Brillouin spectra do not show significant differences between the smectic- C^* and the smectic- A phases: the polarization selection rules are not modified and both QL and QT modes are observed with intensities comparable with those obtained in the A phase. A more careful investigation indicates a reproducible small anomaly in C_{33} near the smectic- C^* -smectic- A transition at T_{AC} (Fig. 4). A similar very weak anomaly for C_{11} seems to be present but, due to the experimental errors, it is doubtful. It should be noted that the evaluation of C_{13} is possible only from complete anisotropy measurements (like those presented in Fig. 3) while the values of C_{11} or C_{33} can be obtained by a direct measurement for $\varphi=90^\circ$ or $\varphi=0^\circ$ and all their temperature dependence can be measured in a single pass without moving the sample. Thus the accuracy of the determination of the relative variation for C_{11} and C_{33} is much better than that for C_{13} . Therefore we cannot conclude whether the small increase observed for C_{13} near T_{AC} is due to transition effects or that it is only an artifact.

The tilt angle θ between the z axis and the director is the order parameter for this second-order phase transition: one expects a coupling between θ^2 and the longitudinal strains,

giving rise to steplike anomalies in the stiffness constants C_{11} and C_{33} . Most probably this anomaly is smeared at the hypersonic Brillouin regime: the frequency of the amplitude mode related to the fluctuations of the tilt angle θ is much lower (of the order of 10^5 Hz).

Finally some spectra were recorded using an applied dc electric field in order to unwind the helical structure of the C^* ferroelectric phase. The observed changes around T_{AC} are extremely small and the experimental uncertainties do not allow one to make conclusions about the influence of the dc field.

C. Discussion

Let us analyze briefly the hydrodynamic approach that was used previously to discuss the results in smectic- A phases [23,24]. As mentioned in the Introduction, for the smectic crystals the hydrodynamic approach [1,4] allows us to justify the phenomenological analysis used in Sec. III B. The classical equations of motion found for an isotropic liquid are modified by introducing an additional variable u that describes the layer displacement and provides the following contribution to the free energy:

$$F_u = \frac{1}{2} \Phi_3 \left(\frac{\partial u}{\partial z} \right)^2 + \frac{1}{2} \Phi_1 \left(\frac{\partial^2 u}{\partial x^2} + \frac{\partial^2 u}{\partial y^2} \right)^2 + \frac{1}{\rho_0} \sigma_{\rho\rho} \frac{\partial u}{\partial z} + \frac{1}{T_0} \sigma_T T \frac{\partial u}{\partial z}, \quad (12)$$

where ρ and T stand for density and temperature fluctuations and ρ_0 and T_0 for their equilibrium values, respectively. The dynamics are described by six linearized equations of motion:

$$\begin{aligned} \dot{\rho} &= -\rho_0 \partial_i v_i, \\ T_0 \dot{s} &= \kappa_{ij} \partial_{ij} T + \mu \partial_{zj} \sigma_{jz}, \\ \dot{u} &= v_z + \frac{\mu}{T_0} \partial_z T + \xi \partial_j \sigma_{jz}, \\ \rho_0 \dot{v}_i &= -\partial_i p + \delta_{iz} \partial_j \sigma_{jz} + \eta_{ijkl} \partial_{jl} v_k, \end{aligned} \quad (13)$$

σ_{jz} is a mechanical stress associated with the derivatives of the displacement u , s is the density of entropy, v_i are the components of the velocity, η_{ijkl} are the coefficients of the viscosity tensor with appropriate symmetry (cf. above), κ_{ij} are the components of the thermal conductivity tensor, and μ , ξ are other phenomenological coefficients. Replacing s , σ_{jz} , and the hydrostatic pressure p by linear combinations of T , ρ , and derivatives of u [3], one finds, in addition to diffusive solutions, the propagating modes phenomenologically described in Sec. III B 1 with the following stiffness constants:

$$\begin{aligned} C_{11} &= C_0 \\ &= \rho_0 \left(\frac{\partial p}{\partial \rho} \right): \text{value obtained for the isotropic liquid,} \end{aligned} \quad (14)$$

$$C_{13} = C_0 - \sigma_{\rho},$$

$$C_{33} = C_0 - 2\sigma_\rho + \Phi_3.$$

Assuming that the hydrodynamic model is valid, one can calculate σ_ρ and Φ_3 [cf. Eq. (14)] from the Brillouin experimental data as it was done in several papers [23,24]. In our case σ_ρ and Φ_3 would be found to have the same order of magnitude and would tend continuously to zero when the isotropic phase is approached. However, this interpretation is not satisfactory taking into account the Brillouin data in both nematics and smectics. In the nematic phase there is no hydrodynamic contribution to the elastic anisotropy in contradiction with various experimental results [5,11]. Our experimental results are very close to the previously reported ones concerning nematic liquid crystals. The anisotropy of the stiffness constants in our material only very slightly exceeds the values in nematic 4-cyano-4-*n*-alkylbiphenyles (*n*CB), MBBA, and PAA. For example, 15 °C below the isotropic-mesophase transition, the value of $(\nu_3 - \nu_1)/\nu_1$ is 5.5% of our sample, while most of the previously studied nematic compounds show an anisotropy between 3% and 4% [5]. In our sample the anisotropy of the viscosity coefficients $(\eta_{33} - \eta_{11})/\eta_{11}$ (35%) is of the same order of magnitude as, for instance, in MBBA or PAA (about 30%). Moreover, in the temperature range neighboring the isotropic-smectic phase transition the behavior of the QL propagation mode is analogous to that observed in the vicinity of the isotropic-nematic transition regarding both the continuous increase of the velocity anisotropy and the abrupt jump of the viscosity. In the isotropic-nematic phase transition the viscosity also seems to be the most affected quantity as in the isotropic-smectic transition. The common property of the smectic and nematic phases is the orientational order of the molecules. Thus, the viscosity looks to be very sensitive to the orientations of molecules and not to the layer structure. On the other hand, differences between nematics and smectics have been detected in the ultrasonic regime where the reported elastic stiffness anisotropy is very weak in nematics, while it is generally clearly present in smectic structures.

The hydrodynamic theory fails when an additional low-frequency quantity (for example, some slow relaxational mechanism) couples to the hydrodynamic variables. The corresponding equation of motion has to be incorporated to the system of Eqs. (13) and the dynamics of ρ and u can be strongly modified. Consequently, the values of C_{ij} from Eq. (14) are renormalized. Relaxation phenomena due to intramolecular degrees of freedom were observed in many organic liquids [25]. In nematic liquid crystals [26] a single relaxation process (with a relaxation frequency in the MHz range) was attributed to the *trans-gauche* rotation isomerism of the molecule end chains. A high-frequency relaxation behavior (in the GHz range) was also revealed in nematic liquid crystals [11]. A relaxation in a similar frequency region (called β relaxation) was observed in ferroelectric liquid crystals [27,28] by dielectric spectroscopy and was assigned to the libration (hindered rotation) of the molecule around its long axis. It has to be pointed out that the two latest relaxation mechanisms show the same frequency range and very small temperature dependence.

It then seems that a general relaxation mechanism is present in both smectic and nematic liquid crystals giving a significant contribution to the elastic anisotropy. The effect

of the hydrodynamic terms [Eq. (14)] gives account, at least partially, for the ultrasonic anisotropy [14]. However, in the hypersonic range, the hydrodynamic contribution is probably smaller than (or at most comparable to) that related to the above-mentioned relaxation mechanism. In order to evaluate the hydrodynamic terms, it would be necessary to perform an experimental study within a broad frequency range for the same smectic liquid crystal.

As to the intensity interpretation, one can suppose that this additional relaxational process only weakly affects the coupling between ρ and u on one hand and the high-frequency permittivity fluctuations on the other hand. This means that it is possible to analyze the photoelastic coefficients in terms of the hydrodynamic theory. When deriving the expression for the scattered intensity, one has to realize that the density fluctuations correspond to the volume changes, i.e., $e_{11} + e_{22} + e_{33}$ in terms of deformations and that the derivative of the displacement $\partial u/\partial z$ can be assigned to e_{33} . Then, we can write the change of the free energy related to the high-frequency permittivity modulation in terms of only two independent strains ($e_{11} + e_{22} + e_{33}$) and e_{33} :

$$\Delta F = [(E_1^2 + E_2^2)p_{1\rho} + E_3^2 p_{3\rho}](e_{11} + e_{22} + e_{33}) \\ + [(E_1^2 + E_2^2)p_{1u} + E_3^2 p_{3u}]e_{33},$$

where E_i are the components of the electric field and $p_{i\rho}$, p_{iu} are appropriate photoelastic coefficients which form the non-zero part of the matrix p_{ij} :

$$p_{ij} = \begin{pmatrix} p_{1\rho} & p_{1\rho} & p_{1\rho} + p_{1u} \\ p_{1\rho} & p_{1\rho} & p_{1\rho} + p_{1u} \\ p_{3\rho} & p_{3\rho} & p_{3\rho} + p_{3u} \end{pmatrix}.$$

Thus, our supposition that $p_{13} \approx p_{11}$ and $p_{31} \approx p_{33}$ means, in the language of hydrodynamics, that the contribution of u to the scattered intensity is much smaller than the contribution of ρ . This hypothesis is justified by the fact that u is a morphic variable in the smectic-A phase. Experimentally, we found that p_{11} is slightly larger than p_{13} and smaller than p_{31} ; p_{1u} and $p_{1\rho}$ then show opposite signs with $|p_{1u}| \ll |p_{1\rho}|$. From the experimental values obtained at 33 °C one can estimate

$$p_{1\rho}/p_{3\rho} \approx 0.95,$$

$$p_{1u}/p_{1\rho} \approx -0.2.$$

This means that $p_{1\rho}$ and $p_{3\rho}$, which are identical in the isotropic phase, stay close to each other in the smectic phases. The morphic coefficient p_{1u} is smaller. If the second morphic coefficient p_{3u} behaves analogously, which means $p_{1u} \approx p_{3u}$, one obtains the following inequality: $p_{13} < p_{33} < p_{31}$. Due to the decrease of p_{33} , the right part ($\varphi > \varphi_L$) of the QT-intensity curve [Figs. 2 and 10(b)] is further reduced and the influence of p_{11} on the QL-intensity curve is compensated. Unfortunately, we cannot compare our results with other liquid crystals because there are no experimental data in the literature concerning the Brillouin scattering intensities in such compounds.

Considerable effort was made to detect the QT mode in classical nematics [5], but the corresponding Brillouin line

was not experimentally found. It has been suggested that this mode should be overdamped in such structures. In our opinion, it is possible to envisage also another explanation of the experimental results reported in [5]: the frequency and the intensity of the QT mode are probably very low. It follows from our study that the QT mode is not easily resolved for 45° (angle used in [5]): its intensity is already very low. It is not clear whether one can introduce, even in nematics, some coefficients analogous to p_{1u} and p_{3u} and, in such a hypothesis, what are their magnitudes. However, the importance of p_{1u} is clear: without its small contribution the intensity of the QT mode in our sample would be two or three times lower [cf. Fig. 10(b)]. In addition, the velocity of the QT mode (~ 300 m/s) in the studied nematic materials (nCB) is lower than that in our sample (~ 500 m/s). It then follows that the QT mode can be undetectable by means of scattering experiments in these materials. We believe that the results of the pseudocrystalline model are applicable to both QL and QT modes in the smectics as well as in the nematics.

IV. CONCLUSION

In this paper we reported a complete set of Brillouin data in smectic- A and smectic- C^* phases. A weak quasitrans-

verse mode was observed in a limited angular range well below the isotropic–smectic- A phase transition.

The results were interpreted in the frame of a phenomenological model that is usually used for the description of elastic properties in solid crystals. We extended the model by applying it equally to the calculations of the scattered intensity. The results experimentally obtained for the QL and the QT modes are coherent with the predictions of the model. Using the data relative to the QL mode the model successfully fits the characteristics of the QT mode. Thus we showed that the model is fully applicable to liquid crystals.

The behavior of the real and imaginary part of the stiffness tensor in the smectic phases is similar to that found in nematics and is probably related to a general relaxation mechanism in the GHz frequency range. The anomalies found at the smectic- A –smectic- C^* phase transition are very weak: the frequency of the soft mode is too low to be detected by our technique.

ACKNOWLEDGMENTS

The authors are indebted to R. Dabrowski and H. Sverenyák for preparing the studied samples and to M. Glogarová and V. Dvořák for helpful discussions.

-
- [1] P. C. Martin, O. Parodi, and P. S. Pershan, *Phys. Rev. A* **6**, 2401 (1972).
 - [2] H. R. Brand and H. Pleiner, *J. Phys. (Paris)* **45**, 563 (1984).
 - [3] P.-G. de Gennes and J. Prost, *The Physics of Liquid Crystals* (Clarendon, Oxford, 1993).
 - [4] K. Miyano and J. B. Ketterson, *Sound Propagation in Liquid Crystals, in Physical Acoustics*, edited by W. P. Mason and R. N. Thurston (Academic, New York, 1979), Vol. 14, pp. 93–178.
 - [5] J. K. Krüger, C. Grammes, R. Jiménez, J. Schreiber, K.-P. Bohn, J. Baller, C. Fischer, D. Rogez, C. Schorr, and P. Alnot, *Phys. Rev. E* **51**, 2115 (1995).
 - [6] D. G. Gleed, J. R. Sambles, and G. W. Bradberry, *Phys. Lett. A* **134**, 440 (1989).
 - [7] Y. Liao, N. A. Clark, and P. S. Pershan, *Phys. Rev. Lett.* **30**, 639 (1973).
 - [8] K. A. Kemp and S. V. Letcher, *Phys. Rev. Lett.* **27**, 1634 (1971).
 - [9] D. Eden, C. W. Garland, and R. C. Williamson, *J. Chem. Phys.* **58**, 1861 (1973).
 - [10] S. Bhattacharya, B. K. Sarma, and J. B. Ketterson, *Phys. Rev. Lett.* **40**, 1582 (1978).
 - [11] C. Grammes, J. K. Krüger, K.-P. Bohn, J. Baller, C. Fischer, C. Schorr, D. Rogez, and P. Alnot, *Phys. Rev. E* **51**, 430 (1995).
 - [12] K. Miyano and J. B. Ketterson, *Phys. Rev. A* **12**, 615 (1975).
 - [13] A. E. Lord, *Phys. Rev. Lett.* **29**, 1366 (1972).
 - [14] K. Miyano and J. B. Ketterson, *Phys. Rev. Lett.* **31**, 1047 (1973).
 - [15] D. Collin, J. L. Gallani, and P. Martinoty, *Phys. Rev. Lett.* **61**, 102 (1988).
 - [16] J. Pavel, M. Glogarová, and R. Dabrowski, *Ferroelectrics* **81**, 413 (1988).
 - [17] J. M. Vaughan, *Phys. Lett. A* **58**, 325 (1976).
 - [18] J. K. Krüger, A. Marx, L. Peetz, R. Roberts, and H.-G. Unruh, *Colloid Polym. Sci.* **264**, 403 (1986).
 - [19] P. Kužel, V. Dvořák, and P. Moch, *Phys. Rev. B* **49**, 6563 (1994); P. Kužel, PhD. thesis, Université Paris-XIII, 1994 (unpublished).
 - [20] I. L. Fabelinskii, *Molecular Scattering of Light* (Plenum, New York, 1968), Chap. IX, p. 139.
 - [21] R. Vacher and L. Boyer, *Phys. Rev. B* **6**, 639 (1972).
 - [22] F. Brochard, *Phys. Lett. A* **49**, 315 (1974).
 - [23] G. W. Bradberry and J. M. Vaughan, *Phys. Lett.* **62A**, 225 (1977).
 - [24] A. Wergin, W. Krasser, H. H. Stiller, and C. G. B. Frischkorn, *Phys. Rev. A* **20**, 1120 (1979).
 - [25] K. F. Herzfeld and T. A. Litovitz, *Absorption and Dispersion of Ultrasonic Waves* (Academic, New York, 1959).
 - [26] S. Nagai, P. Martinoty, and S. Candau, *Mol. Cryst. Liq. Cryst.* **31**, 243 (1975).
 - [27] A. Schönfeld, F. Kremer, and R. Zentel, *Liq. Cryst.* **13**, 403 (1993).
 - [28] A. Schönfeld and F. Kremer, *Ber. Bunsenges. Phys. Chem.* **97**, 1237 (1993).